A. J.			
Amrit Journal	October, 2025	Volume 5, Issue 1	ISSN: 2594-3235

Pristine Lead Oxide Nanocatalyst for Photolytic, Photothermal and Dark Medium Degradation of Murexide

Shukra Raj Regmi[1]*, Nurul Hoda Khan[1], Narendra Prakash Shawd[1], Dikpal Kumar Shahi[1], Lekha Nath Khatiwada[2], Rishi Ram Ghimire[3], Rameshwar Adhikari[4]*

[1]Graduate School of Science and Technology, Mid-West University, Surkhet, Nepal

[2]Department of Customs, Ministry of Finance, Tripureshwar, Kathmandu, Nepal

[3]Department of Physics, Patan Multiple Campus, Tribhuvan University, Nepal

[4]Research Centre for Applied Science and Technology (RECAST), Tribhuvan University, Kirtipur, Kathmandu 44618, Nepal

*Corresponding author; *shukra.regmi@mu.edu.np* (https://orcid.org/0009-0003-5844-4448), *nepalpolymer@yahoo.com* (https://orcid.org/0000-0002-7350-0204).

Received: 8 July 2025; Received in revised form: 30 September 2025; Accepted: 7 October 2025

Abstract

Lead oxide nanocatalyst (PbO-NC) is synthesized by the co-precipitation to evaluate its photolytic, photothermal, and dark medium catalytic performance under controlled laboratory conditions. The catalyst is characterized by UV-visible spectroscopy, FTIR, EDX, and XRD techniques; the band gap obtained at 3.70 eV. XRD indicated a tetragonal phase with an average size of 21 nm, and crystallinity of 50.27%. The PbO-NC effectively degraded ammonium purpurate (murexide) under normal solar irradiance (6.91±0.38 kWh/m^2/day) with a high-rate constant, i.e., 0.0154 min^{-1} in light, 0.00412 min^{-1} in dark, and 0.0158 min^{-1} in photothermal degradation. The obtained result is higher than other type of oxide-based pure nanocatalytic degradation, and the catalyst is readily recoverable. The catalytic degradation in all circumstances obeyed pseudo-first-order kinetics and efficiencies of 98%, 88%, and 38% in photolytic, photothermal, and dark conditions. Although the synthesis of PbO-NC is tedious and involves toxic precursors, the photosensitive and photothermal properties make it a promising catalyst for degrading heavily toxic dyes.

Keywords: *Lead oxide nanocatalyst, photolytic, photothermal, dark medium degradation, co-precipitation, catalytic efficiency*

1. Introduction

Murexide is a purine derivative used as a common metal complexing agent in analytical chemistry due to its sharp purple color [1-3]. It is widely applied in paint and textile industry for coloring and in analytical chemistry for the estimation of rare earth, calcium, nickel, and magnesium metals. Report shows that the excess contamination may cause mutagenicity and nephrotoxicity, but it is not classified as a major carcinogenic agent for human health [4]. It contains alloxantin with nitric acid and ammonia, considered as a stable organic dye having the molecular formula $C_8H_8N_6O_6$ [5]. Murexide-metal complex can be easily distinguished as a potential source of water contaminant due to its sparingly soluble nature in cold water [1-3].

Organic dyes, including murexide, can be degraded photolytically and photothermally by oxide based nanocatalyst. In the present work, we have synthesized lead oxide nanocatalyst by the co-precipitation method under the controlled laboratory parameters [6-10]. Like ZnO, TiO_2, SnO_2, Fe_2O_3 and CuO, the lead oxide nanocatalyst (PbO-NC) shows strong photocatalytic property [11-13]. The crystalline PbO-NC exist in tetragonal (litharge) and orthorhombic (massicot) having unique optical band gap 2.3-3.1 eV [4, 14]. The yellow color PbO-NC has a high surface area to volume ratio (50-150 m^2/g), which makes it sensitive to photocatalytic and photothermal reactions. Lead oxide nanocatalyst can be prepared by varieties of technique; among them facile chemical precipitation gives low cost size variable particles, sol-gel method provides highly pure and uniform particles, and green synthesis is achieved by using natural plant extract as a capping agent [8-10, 15].

Angel N.L. (2023) reported that efficient photocatalytic degradation (~95%) of nuclear red dye is achieved by tetragonal PbO-NPs under UV light as a promising photocatalyst in wastewater treatment [16]. Kumar A., et al. (2020) reported the synthesis of nickel dopped PbO that shows effective degradation of methylene blue and mineralization via COD reduction supported by physiochemical characterization [17]. Borhade A.V. (2012) reported the rhombic structure PbO-NPs having size 41 nm with 4.28 eV band gap could degrade methylene blue obeying pseudo-second order kinetics. Feng Pan. (2023), reported the composite membrane based on lead oxide (20%) showed ~71% congo red degradation within 50 minutes, showing effective wastewater treatment in photolight [18]. Elango G., (2015), reported the plasmon excited Pb-NPs having size 47 nm, which degrades malachite green at 254 nm effectively [19].

Fikadu T.G. (2023) reported the complete degradation of methylene blue by Sn-doped α-PbO under solar light, demonstrating the enhanced catalytic activity over the pristine α-PbO [20]. Rauf, M. A. et al. (2009) reported the synthesis of Pb-NPs for the degradation of dye through adsorption, sedimentation for water treatment in agriculture, and domestic use [20]. Nasir. G. (2024) reported the biosynthesized PbO-NPs through mulberry leaf extract remove 99.9% dye of 100 ppm concentrations at pH 10 in 30 minutes [21]. Gaber M. (2012) reported the PbO based electrodes, which degrades 95 % yellow 160 dye within 15 minutes at pH 7.13 at 25^oC showing high efficiency for wastewater treatment [22]. Wang Z. (2019) reported that 20 μM benzophenone-3 is effectively

degraded by 0.75 g/L of PbO/TiO_2 composite under UV-C light at pH 7, obeying pseudo-first-order kinetics [23].

The review reports showed that there is no solid evidence for the murexide degradation by the lead oxide nanocatalyst. Some reports claim that murexide forms a stable bond with lead, and its adsorption takes place on the surface of the particle [24, 25]. In the present work, our rationale is to make a foundation through the study of photocatalytic and photothermal degradation of murexide at different time and temperatures. However, lead oxide nanomaterial is not a safe and preferable catalyst for the photolytic and photothermal degradation of dye due to its potential toxicity; the opto-electronic behavior of PbO-NC cannot be undermined in dye degradation application for relative comparison with other potential catalyst. The present work is carried out only for the quantitative determination of catalytic strength of PbO-NC on murexide degradation instead of existing and preferable catalyst commonly used in the dye degradation process.

2. Materials and Methods

2.1 Chemicals

All chemicals used in the experiment were ultrapure spectroscopic grade. Lead acetate ($(CH_3COO)_2Pb.3H_2O$, M.W = 379.33 g/mol, CAS No. 6080-56-4, ≈ 99%) was purchased from Fisher Scientific, India. Ammonium purpurate ($C_8H_4N_5O_6NH_4$, M.W = 284.19 g/mol, CAS. No. 3051-09-0) was purchased from Thermo Fisher Scientific India. Sodium hydroxide (NaOH, 40 g/mol, CAS No. 1310-73-2, 97 %) was purchased from Qualigen, India. Polyethylene glycol (PEG, $H\text{-}(O\text{-}CH_2\text{-}CH_2)_n\text{-}OH$, 100 g/L, CAS No. 25322-68-3) was purchased from Merc, India. Ethanol (C_2H_5OH, 99.99 %, 46.06 g/mol, CAS No. 64-17-5) was purchased from Fusion Biotech, India.

2.2 Synthesis of lead oxide nanocatalyst (PbO-NC)

Initially, 0.1 M Lead (II) acetate trihydrate precursor was made by dissolving 37.93 g on 1 L deionized distilled water. 1 M NaOH was prepared by dissolving 40 g pallets in 1 L deionized distilled water. The precursor solution was stirred for 1 hour in 250 rpm at 25^{o}C, which was followed by adding alkali dropwise from the burette until the pH of the solution maintained exactly at 10. While adding NaOH, the precipitation process was controlled by adding 5 mL polyethylene glycol (PEG) slowly in the solution with the help of syringe. The precipitation was completed in 2 hours of constant stirring. The solution was kept for 1 hour in a probe sonicator, which was latter kept at 60^{o}C for aging for 24 hours in a hot air oven. The complete evaporation left a white crystalline powder, which was calcined in a muffle furnace at 400^{o}C for 3 hours. The obtained lead oxide crystalline power was stored in an airtight bottle, which was used as lead oxide nanocatalyst (PbO-NC) in the experiment [26, 27].

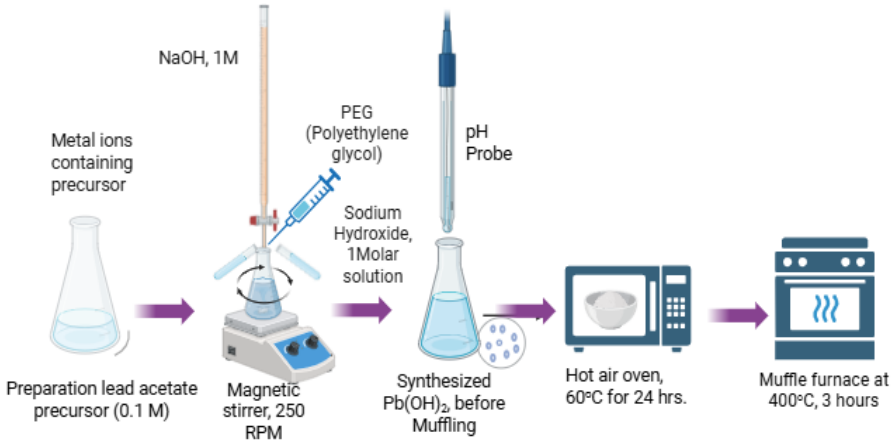

Fig. 1. Synthetic pathway for Lead oxide nanocatalyst by co-precipitation method.

2.3 Characterization of lead-oxide nanocatalyst (PbO-NC)

Lead oxide nanocatalyst was characterized by an UV-visible spectrophotometer (UV-1900i, Shimadzu, Japan) to obtain the maximum absorption wavelength of the particle. The bonding nature between lead and oxygen was determined by Fourier Transform Infrared Spectroscopy (FT-IR, IR Affinity-1s, Shimadzu, Japan). The elemental composition in the catalyst was determined by Energy Dispersive X-Ray (EDX-8000, Shimadzu, Japan). The crystallography and indices were determined by XRD (Bruker, D2 Phaser, Massachusetts, USA). The geometric structure was obtained from the simulation technique using VESTA.

2.4 Photointensity measurement

The experiment was carried out in the month of May (11:00 am morning to 2:00 pm day)-2025. The solar intensity was measured by CMP3 Pyranometer. The light intensity was recorded highest on 2nd day of May, and lowest recorded on the 29th. The average solar intensity distribution was found to be 6.91±0.38 kWh/m^2/day. The experimental data were recorded based on average solar intensity distribution.

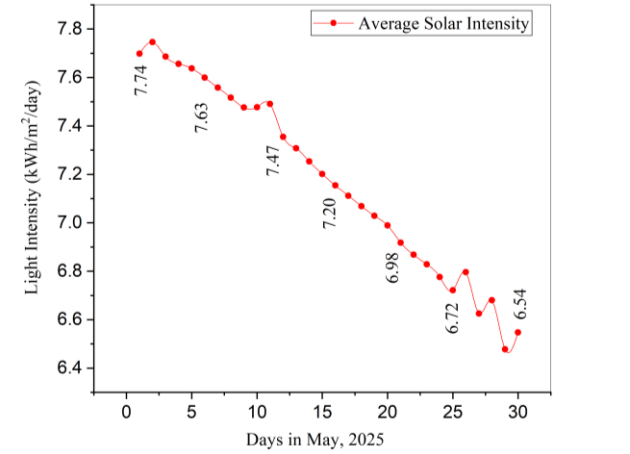

Fig. 2. Distribution of daily solar intensity average in May-2025 (11:00 am-2:00 pm) measured by CMP3 Pyranometer, Gurashe, Surkhet, Karnali province, Nepal.

2.5 Langmuir-Hinshelwood model

Heterogeneous catalytic reaction model explains the photocatalytic degradation mechanism. The adsorption or photocatalytic degradation and particle desorption is explained by the following equation [45, 46].

$$r = \frac{kKC}{1+kC} \qquad \ldots(i)$$

Where, 'r' is the degradation rate in $mgL^{-1}min^{-1}$, 'k' represents the reaction rate in min^{-1}, 'K' denotes the Langmuir adsorption constant in Lmg^{-1}, 'C' is the substrate concentration in mgL^{-1}. The linearized photocatalytic kinetics can expressed as:

$$\frac{C}{r} = \frac{1}{kKC} + \frac{1}{k} \qquad \ldots(ii)$$

Where, slope = $1/kK$, Intercept = $1/k$.

Similarly, if, KC << 1, 1 + KC ≈ 1, pseudo first –order-kinetic model can be explained as:

$$ln\frac{C_o}{C_t} = kt \qquad \ldots (iii)$$

Where, 'C_o' is the initial concentration and '$C_{t'\ is}$ the final concentration, 'k' represents the rate constant, and 't' is the time.

3. Result and Discussion

3.1 UV-visible spectra and Tauc plot

The UV-Visible spectroscopy was used to determine the band gap energy, particle size and electronic transition dependent on quantum effect. The maximum absorption peak was determined by the calibration of device at its optimum level. The absorption peak was obtained at 240 nm, which indicates the quantum confinement effect resulting blue shift compared to the bulk particles [44].

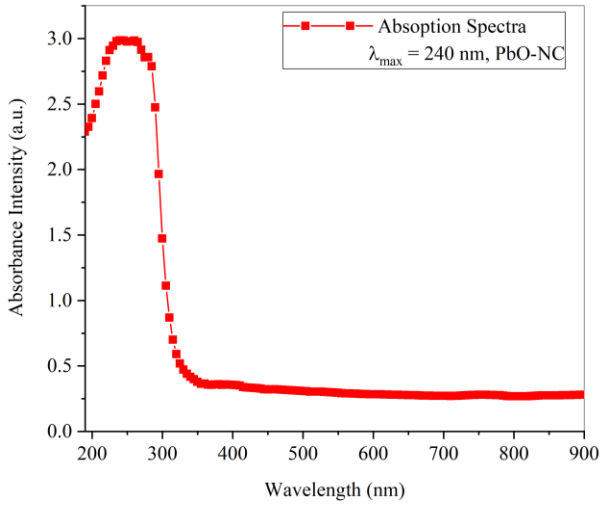

Fig. 3. UV-visible spectra of PbO-NC showing its maximum absorption wavelength.

The UV-visible spectra of PbO-NC in figure 3 reveals that the maximum absorption wavelength at 240 nm, which is approximately equal to the reported value [43]. The wavelength intensity and nature of spectra is affected by the size of particle, solvent effect, pH, temperature and instrumental factors. The hypsochromic shift indicates the pristine PbO-NC directs blue shift due to polar n→π* transition [29]. The strong quantum confinement has made the band gap 3.70 eV with allowed direct band gap.

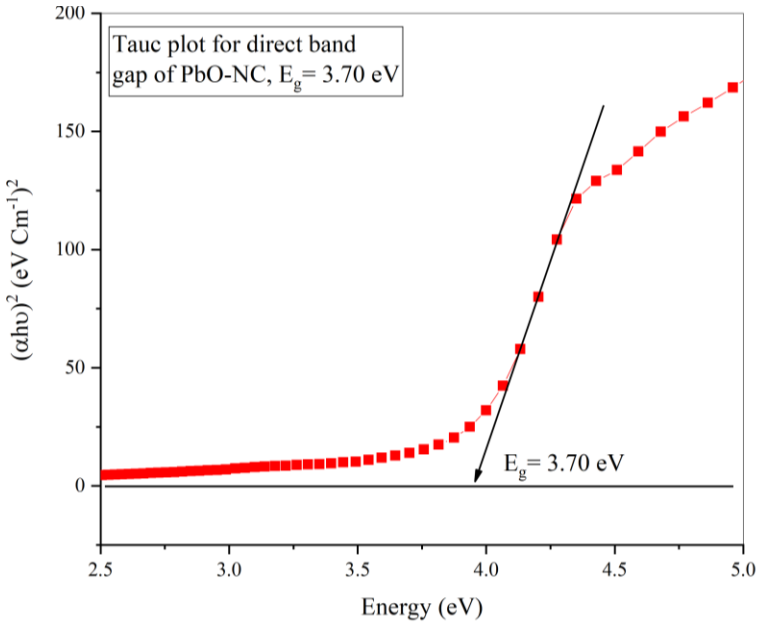

Fig. 4. Tauc plot for the direct band gap of PbO-NC showing optical band gap at 3.70 eV.

The extrapolation of Tauc plot showed the optical band gap at 3.70 eV. The direct allowed transition is calculated as [30]:

$$(\alpha h\nu)^2 = A(h\nu - Eg) \quad \ldots \quad \text{(iv)}$$

The direct transition allowed for n = 2.

The wavelength obtained for PbO-NC is converted into the photon energy as:

$$h\nu = \frac{hc}{\lambda} = \frac{1240}{\lambda} \qquad \ldots \qquad \text{(v)}$$

The obtained values for $(\alpha h\upsilon)^2$ vs. photon energy in eV gives extrapolation of curve intercept along x-axis gives the mathematical values of optical band gap, which is found to be 3.70 eV. The obtained band gap for lead oxide nanocatalyst is approximately equal to the reported band gap. Repots shows that α-PbO having size ~36 nm with direct transition for n = ½ gives band gap at 3.91 eV [31]. Similarly, β-PbO having size ~45 nm with direct transition gives band gap 3.85 eV, and nanomaterials having size 20-30 nm with direct transition shows 2.95 eV band gap [32]. Some reports reveal that PbO nanomaterials obtained under controlled temperature gives band gap at

2.09 eV [33]. The particle nature determines the optical band gap from Tauc plot mainly size and a route through which the particle formed. In the present work, the obtained band gap for PbO-NC through chemical precipitation method reveals crystalline size particles having unique quantum confinement and surface effect.

3.2 Fourier Transform infrared (FTIR) spectroscopic analysis for lead-oxide nanocatalyst (PbO-NC)

FTIR spectra are analyzed to find specific vibrational group present in the catalyst. Figure 5 shows the FTIR spectra of PbO-NC.

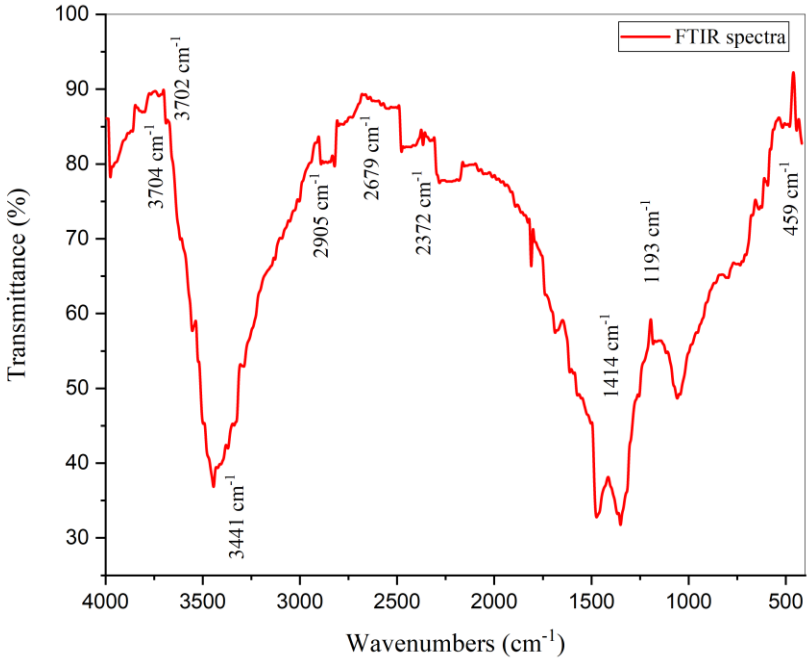

Fig. 5. FTIR spectra of PbO-NC showing strong lead-oxygen stretching.

The FTIR spectra of PbO-NC shows the sharp stretching of Pb-O stretching at 459 cm^{-1}. The additional wavelength with weak stretching found at 1193 cm^{-1} reveals the presence of CO_3^{2-} in the catalyst, probably due to trace contamination of lead acetate precursor. Furthermore, the H-O-H bending observed at 1414 cm^{-1} confirms the presence of water molecules in nanocatalyst. The sharp O-H bending also observed at 3704 cm^{-1}. The stretching of C-O bond in 1000 cm^{-1} is due to the presence of carboxyl group [32, 34].

3.3 Energy dispersive x-ray (EDX) spectroscopic analysis for lead-oxide nanocatalyst (PbO-NC)

EDX method was used to obtain the elemental composition of lead oxide nanocatalyst. The peak obtained are corresponding to the x-ray produced from the excited catalyst when highly energetic electron beam strike on it. Figure 6 shows the EDX spectra of PbO-NC.

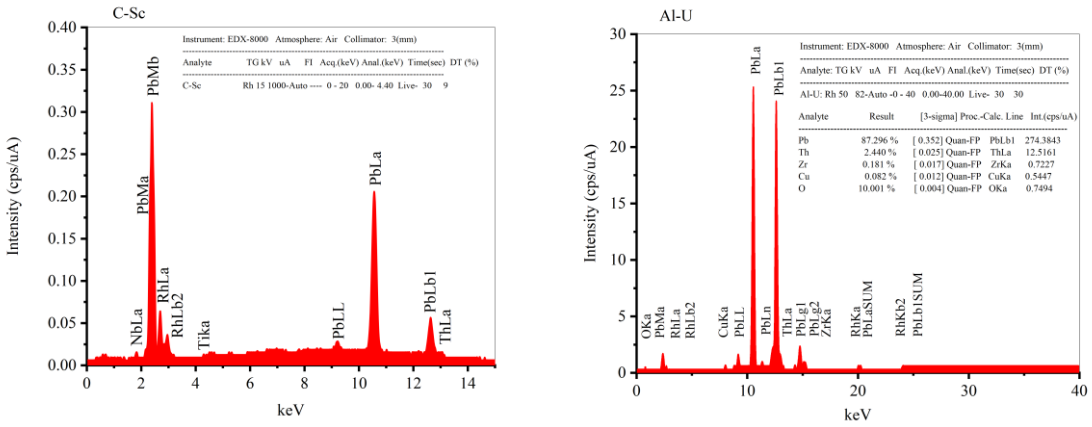

Fig. 6. EDX spectra of PbO-NC showing the elemental composition of lead and oxygen in C-Sc and Al-U mode.

The EDX spectra for PbO-NC revels the elemental composition of lead (Pb) 87.29 % and oxygen (O) 10 %. The spectra also shows the impurities like Thorium (Th) 2.44 %, Zirconium (Zr) 0.18 %, Copper (Cu) 0.082 %. Though the presence of trace concentration in the catalyst decreases the optical band gap, its prominent effect as a catalyst is negligible. Figure (6) shows depicted lead in Lα at 10 KeV, Mα at 2-3 KeV, and Mβ at 12-13 KeV. Similarly, the oxygen Okα is observed at 0.52 KeV. Presence of lead and oxygen in the EDX spectra confirms the existence of PbO nanomaterial [35, 36].

3.4 X-ray diffractometric (XRD) analysis for lead-oxide nanocatalyst (PbO-NC)

The crystallographic indices for PbO-NC show sharp plane at 111, 020, and 220 at their respective diffraction angle 2θ = 30º, 32º, and 36º. The secondary peaks at 002, 310, 113, and 040 represents the presence of impurity in the catalyst. The planes and diffracted angles corresponds to the tetragonal geometry of catalyst [37]. The peak broadening suggests the distribution in size of the particle and crystallinity. On solving Sherrer's equation, we obtained the particle size 21 nm.

$$D = \frac{k\lambda}{\beta \cos\theta} \qquad \text{... (v)}$$

Where, D represents the crystallite size in nm, k is a shape factor, in the present work we found its value 0.9, the wavelength λ for CuKα is 0.15406 nm, β (FWHM) is 0.00684 (≈ 0.39º) radians, and θ = 15º is the Bragg's angle [38]. The peak deconvolution method is used to find out the crystallinity and was found 50.25 % crystalline [39, 40].

$$\text{PbO} - \text{NC Crystallinity} = \frac{\text{Crystallinity in PbO} - \text{NC (a.u)}}{(\text{Crystallinity} + \text{Amorphous})\ (\text{a.u})} x\ 100\%$$

$$= \frac{24717.76}{49165.742} x\ 100 = 50.27\ \%$$

The XRD profiles for lead oxide nanocatalyst is shown in figure 7.

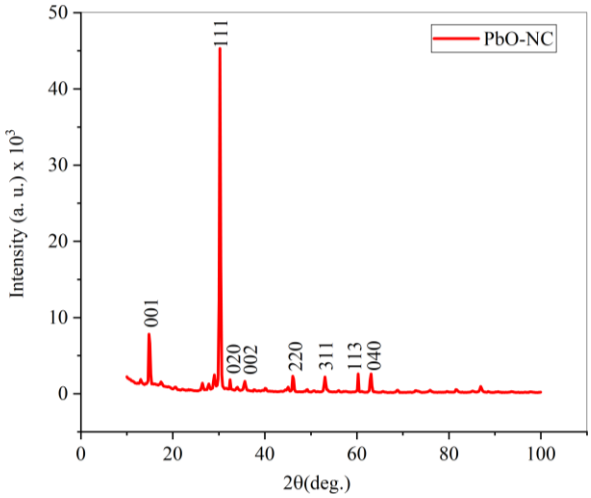

Fig. 7. XRD crystallography of PbO-NC showing their planes in their respective diffractive angles.

Based on the XRD crystallographic planes, and diffractive angles the VESTA simulation predicts tetragonal geometry with interfacial side lengths a = b = c = 3.99000 Å, and interfacial bond angle $\alpha = \beta = \gamma = 90^{o}$. The volume occupied by a single crystal is found to be 5.01000 $Å^3$. The tetragonal PbO-NC is diagrammatically represented in figure 8 [41].

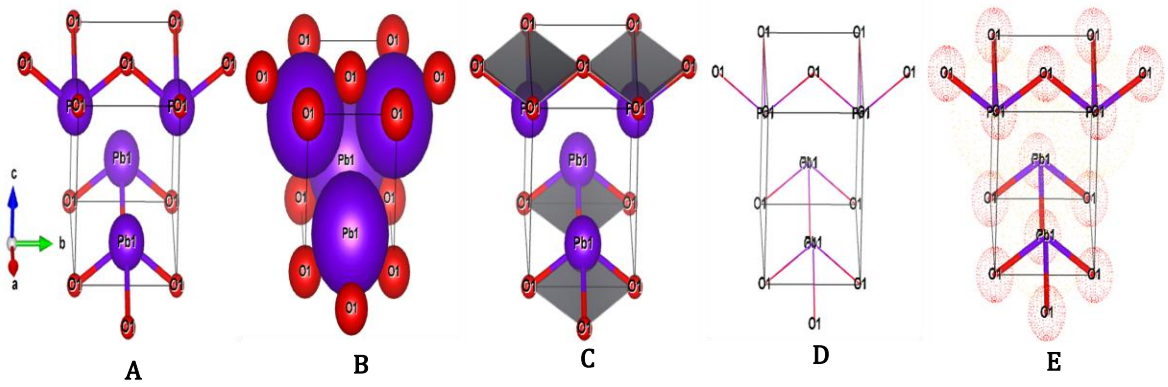

Figure 8. 3D geometric structure of tetragonal PbO-NC showing A) Ball and Stick B) Space Filling C) Tetrahedral D) Wireframe E) Wireframe with density distribution.

3.5 Mechanism of photodegradation of murexide by PbO-NC

Lead oxide is a semiconducting material shows photosensitive nature, which can be tuned by altering the intensity of light. The proposed mechanism shows the solar light absorbed by lead oxide, which excites electrons to the conduction band leaving holes on surface. The photocatalytic degradation mechanism can be explained in the following chemical equations [16, 28].

$$\text{PbO-NC} \xrightarrow{h\nu} \text{PbO } (e^-)_{CB} + \text{PbO } (H^+)_{VB} \qquad \ldots(vi)$$

The hole formed in the catalyst incounter with water molecules that forms hydroxyl ions and rapidly conveted into the powerful hydroxyl free radical.

$$PbO(Hole+)_{VB} + H_2O \rightarrow H^+ + OH^- \text{ (ions)} \quad \ldots(vii)$$

$$PbO(Hole+)_{VB} + OH^- \rightarrow OH\cdot \text{ (radicals)} \quad \ldots(viii)$$

The hydroxyl ions in the solution are converted into the oxygen.

$$4OH^-(Solution) \rightarrow 2H_2O + O_2 \quad \ldots(xi)$$

The free electrons of conducting band reacts with the free oxygen to form very reactive superoxide.

$$PbO(e-)_{CB} + O_2 \rightarrow \cdot O_2^- \text{ (superoxide)} \quad \ldots(x)$$

The formed hydroxide free radicals, and superoxide degrades murexide slowly into their simple compounds.

$$\text{Murexide} + OH^-(Radical) \rightarrow CO_2 + H_2O \quad \ldots(xi)$$

$$\text{Murexide} + O_2^- \rightarrow CO_2 + H_2O \quad \ldots(xii)$$

Low intensity of light and possible recombination of electron hole pair reduces the catalytic efficiency.

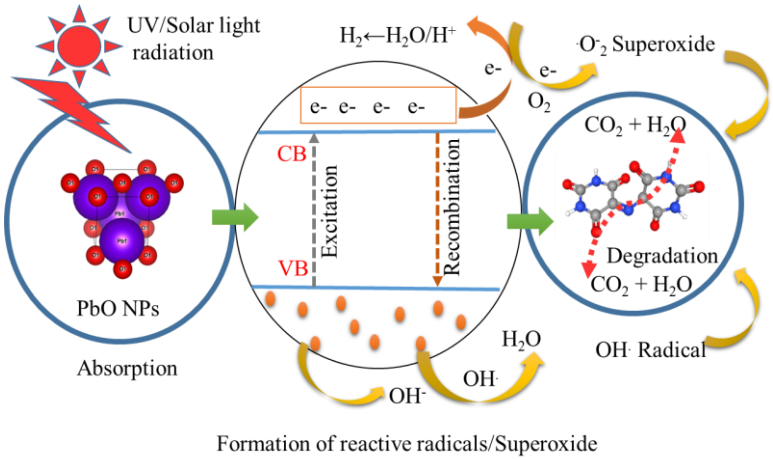

Fig. 9. Schematic diagram for the photosensitization of lead oxide showing formation of hydroxyl free radical and superoxide for the photolytic degradation of murexide dye.

In the present work, a solar light intensity of 6.91±0.38 kWh/m^2/day is used as a photosensitizer. When light absorbs by PbO-NC, the valence electron absorbs light greater or equal to its band gap. The excited electron cross the conduction band leaving behind holes at the surface of the catalyst. The interaction of water with these holes generates hydroxyl ions, which are subsequently converted into the powerful hydroxyl free radicals. Meanwhile, the excited conduction band electrons react with water to form superoxide. The synergistic action of hydroxide and superoxide degrades the murexide continuously until its colour disappears. In contrast, the low intensity solar light promotes the recombination of electron-hole pairs, thereby reducing the catalytic efficiency [42, 43].

3. 6 Photolytic, dark medium and photothermal degradation of murexide

The photocatalytic degradation process was carried out in a borosilicate conical flask by adding 20 ppm murexide prepared in deionized distilled water. Additionally, 20 mg of PbO-NC was introduced into the dye solution, and initial time was recorded. The high dye concentration with a low catalyst amount, or vice versa, does not yield sharp and distinct peaks. Therefore, dye concentration and amount of catalyst were fixed based on the instrumental performance. Upon exposing solution directly to the light, the spectroscopic measurements were initiated. Murexide showed its maximum absorbance at 520 nm. The degradation of murexide concentration was monitored at 10 minutes interval.

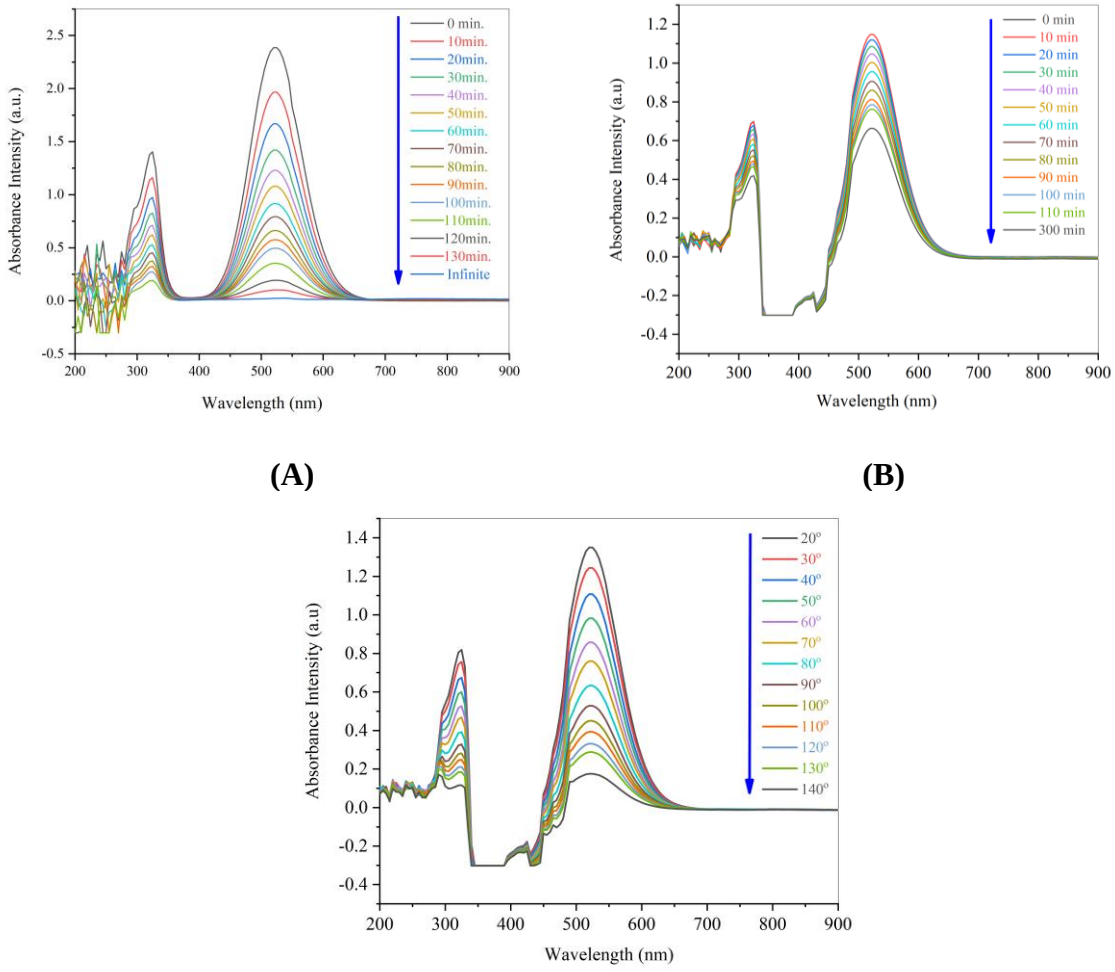

Fig. 10. A) Photodegradation of murexide by PbO-NC showing initial to the infinite time at wavelength 520 nm. B) Catalytic degradation of murexide by PbO-NC in the dark C) Photothermal degradation of murexide by PbO-NC at different temperature.

The process was repeated for the catalytic degradation under identical condition in the dark and the spectrophotometric data were recorded in 520 nm. The photothermal degradation was carried out by repeating the same process under light while tuning temperature from 20^{o}C to 140^{o}C using a hot plate. After complete degradation, the purple colour of murexide completely disappeared, and the solution was centrifuged at 5000 rpm to settle PbO-NC, which remained intact and reusable for multiple degradation cycle.

It was observed that the photocatalytic degradation of murexide completed in 130 minutes, photothermal degradation with tuning temperature completed in 140^{o}C, whereas dark medium degradation incomplete even after 300 minutes, and extended insignificantly to infinity.

In photocatalysis, a monotonic reduction in absorbance intensity at 520 nm indicates the loss of chromophore, which are transformed into spectrally silent intermediates. This occurs due to oxidative cleavage of conjugated bonds by photogenerated reactive superoxide or radicals [15]. In dark medium catalysis, the rapid initial decrease of dye concentration is attributed to the absorption, while negligible degradation occurs with times [47]. In photothermal catalysis, photo light generates electron hole pairs, leading to the production of reactive superoxide and radicals. Simultaneously, thermal energy accelerates the reaction pathway by enhancing the rate of reaction. However, the rate of degradation found in photothermal reaction is lower than photothermal process probably due to electron/hole recombination at 140^{o}C. Notably, complete degradation achieved in photothermal degradation above this threshold.

3.7 Kinetics for the degradation of murexide

The photolytic degradation of murexide by PbO-NC follows pseudo-first-order kinetics. The kinetic plot for $\ln(C/C_o)$ versus time gives a rate constant of 0.0154 min^{-1} with a correlation coefficient (R^2) = 0.999 and Pearson's r = 0.999. Similarly, the kinetic plot for dark medium degradation also obeys pseudo-first-order kinetics with a rate constant of 0.00412 min^{-1}, which is lower than those for photolytic and photothermal degradation. The correlation coefficient (R^2) for dark medium catalysis is 0.973, and Pearson's 'r' = 0.986. Photothermal degradation also obeys pseudo first order kinetics with a rate constant of 0.0158 cm^{-1}. The correlation coefficient (R^2) is 0.973, and the Pearson's r = 0.971. The kinetic plot reveals that the photolytic, and photothermal degradation proceeds with relatively higher rate constant than dark medium degradation of murexide. Figure 11(C, D) shows remaining dye concentration (C/C_o) as a function of time, illustrating progressive dye degradation in light and heat, but not sharply in dark.

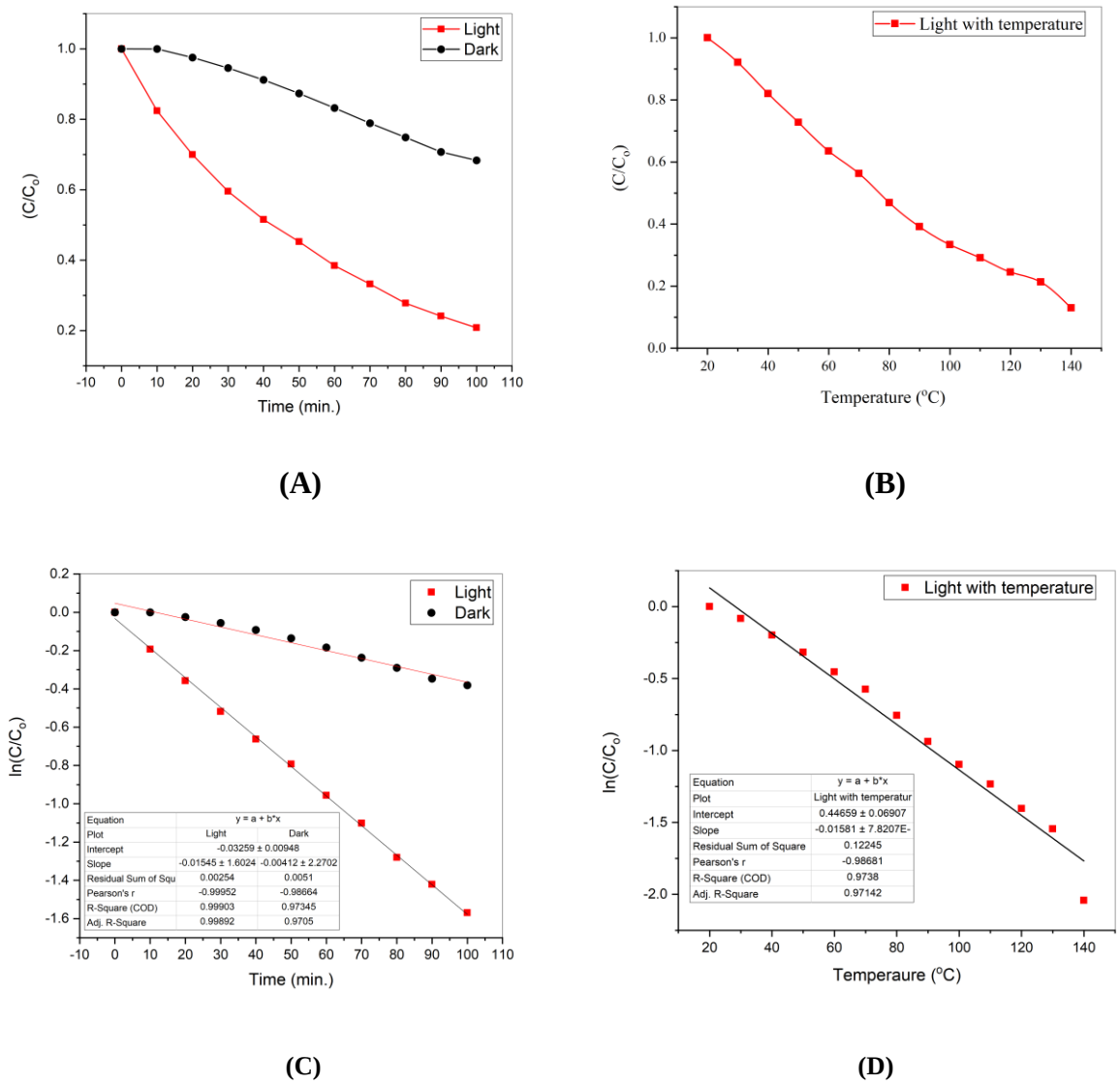

Fig. 11. (A) ln(C/C$_o$) vs. time for light and dark medium degradation, (B) photothermal degradation showing ln(C/C$_o$) vs. temperature, (C) dye concentration degradation showing (C/C$_o$) vs. time, and (D) photothermal degradation showing (C/C$_o$) vs. temperature.

3.8 Catalytic efficiency of lead oxide nanocatalyst (PbO-NC)

The catalytic efficiency of PbO-NC is determined for light, dark, and heat. The catalytic efficiency in light is found 98% in 140 minutes, but in dark medium efficiency is found to be approximately 38 % up to its infinite time. The photothermal degradation shows the catalytic efficiency 88 % in 140 minutes, which is less than the photolytic degradation, probably due to high-energy recombination of excited electrons with holes in the catalyst.

The comparative efficiency is found out:

(PbO-NC)-Light = 98% > (PbO-NC)-Heat & Light = 88% > (PbO-NC)-Dark = 38%

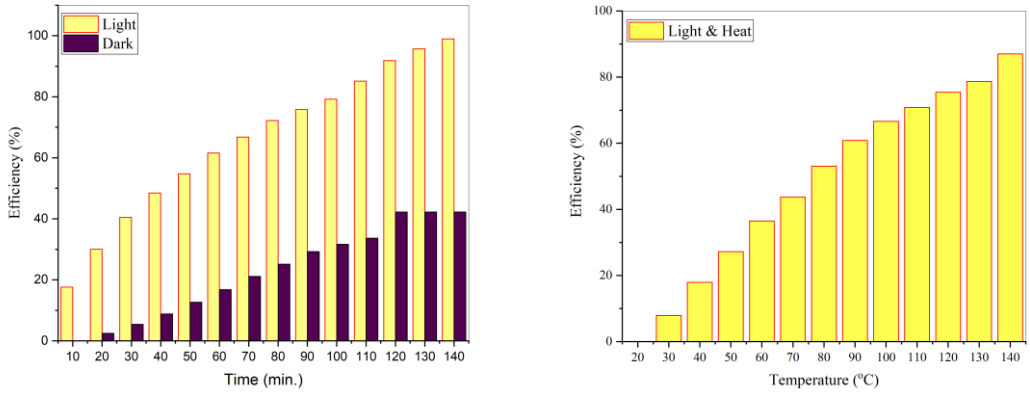

(A) **(B)**

Fig. 12. (A) Catalytic efficiency of PbO-NC in light and dark, and (B) Catalytic efficiency in photothermal degradation.

4. Conclusion

Lead oxide nanocatalyst (PbO-NC) is synthesized through the co-precipitation method to investigate the photolytic, photothermal degradation, and dark medium catalysis of murexide under controlled laboratory conditions. The modern spectroscopic techniques were used to characterize the synthetic nanocatalyst. The UV-visible spectrophotometer revealed that the maximum wavelength absorbance intensity at 240 nm and the obtained Tauc plot revealed the optical band gap at 3.70 eV. The FTIR spectra confirmed the bonding and stretching between lead and oxygen at 459 cm^{-1}. Furthermore, EDX spectra indicated that the catalyst contains lead (Pb, 87%) and oxygen (O, 10%) as an elemental composition. The XRD analysis identified crystallographic indices in 111, 020, and 220 at their respective diffractive angles of $2\theta = 30^{o}$, 32^{o}, and 36^{o}, confirming the existence of tetrahedral phase with a size of 21 nm, and a crystallinity of 50.27 %.

The solar light intensity of 6.91±0.38 $kWh/m^2/day$ was found effective to achieve photolytic, photothermal and dark medium degradation of murexide. The degradation obeys pseudo-first-order kinetics where photolytic degradation showed a rate constant of 0.0154 min^{-1}, and complete degradation obtained in 130 minutes with 98 % catalytic efficiency. Similarly, photothermal degradation showed the rate constant 0.0158 min^{-1} which is completed in 140 minutes with 88% catalytic efficiency. The photothermal degradation of murexide is found to be higher and faster than photolytic and dark medium degradation. Therefore, lead oxide nanocatalyst can serve as an effective catalyst for degrading of complex organic dye.

Acknowledgement

Authors would like to acknowledge the Nanotechnology Laboratory- RECAST, Tribhuvan University, and Central Department of Biological and Chemical Science, Mid-West University, Surkhet, Nepal for laboratory facility.

CRediT authorship contribution statement

Conceptualization, methodology, and investigation: SRR. The experimental set up, material collection, and data analysis: NHK, NPS and DKS. Nanocatalyst characterization and interpretation: LNK. Proofreading, writing: SRR, and RRG. Supervision, manuscript editing, and final draft: RA.

Conflict of interest

Authors declare no conflict of interest.

Availability of data and materials

Data will be provided when requested at chemistry.gsst@mu.edu.np.

References

[1] Masoud, M., Kassem, T., Shaker, M., Ali, A. (2006). Studies on transition metal murexide complexes. *J Therm Anal Calorim*, **84**(3), 549–55. (DOI: https://doi.org/10.1007/s10973-005-9991-3)

[2] Sánchez-Viesca, F., Gómez, R. (2019). On the mechanism of the murexide reaction. *World J Org Chem*, **7**(1), 14–8. (DOI: https://doi.org/10.12691/wjoc-7-1-3)

[3] Abdel-Kader, M. M., Tahoon, K. K., El-Sharkawy, A. (1993). Thermophysical properties of ammonium purpurate "Murexide" C8H4O6N5· NH4. *Phys status solidi*, **135**(1), 161–8. (DOI: https://doi.org/10.1002/pssa.2211350112)

[4] Bratovcic, A. (2020). Synthesis, characterization, applications, and toxicity of lead oxide nanoparticles. *Lead Chem*, 10.

[5] Bürgi, H. B., Djurić, S., Dobler, M., Dunitz, J. D. (1972). Structure and spectra of murexide and of alkali purpurates: Crystal structure of lithium purpurate dihydrate. *Helv Chim Acta*. **55**(5), 1771–82. (DOI: https://doi.org/10.1002/hlca.19720550537)

[6] Eaton, P., Quaresma, P., Soares, C., Neves, C., De Almeida, M. P., Pereira, E. (2017). A direct comparison of experimental methods to measure dimensions of synthetic nanoparticles. *Ultramicroscopy*, **182**, 179–90. (DOI: https://doi.org/10.1016/j.ultramic.2017.07.001)

[7] Dhand, C., Dwivedi, N., Loh, X. J., Ying, A. N. J., Verma, N. K., Beuerman, R. W. (2015). Methods and strategies for the synthesis of diverse nanoparticles and their applications: a comprehensive overview, *Rsc Adv*, **5**(127), 105003–37.

(DOI: https://doi.org/10.1039/C5RA19388E)

[8] Nguyen, T. D. (2013). From formation mechanisms to synthetic methods toward shape-controlled oxide nanoparticles, *Nanoscale*, **5**(20), 9455–82. (DOI: https://doi.org/10.1039/C3NR01810E)

[9] Panigrahi, S., Kundu, S., Ghosh, S., Nath, S., Pal, T. (2004). General method of synthesis for metal nanoparticles. *J nanoparticle Res*. **6**(4), 411–4. (DOI: https://doi.org/10.1007/s11051-004-6575-2)

[10] Ramanathan, S., Gopinath, S. C. B., Arshad, M. K. M., Poopalan, P., Perumal, V. (2021). Nanoparticle synthetic methods: strength and limitations. *Nanoparticles in Analytical and Medical Devices. Elsevier*, 31–43. (DOI: https://doi.org/10.1016/B978-0-12-821163-2.00002-9)

[11] Akter, J., Sapkota, K. P., Hanif, M. A., Islam, M. A., Abbas, H. G., Hahn, J. R. (2021). Kinetically controlled selective synthesis of Cu2O and CuO nanoparticles toward enhanced degradation of methylene blue using ultraviolet and sun light. *Mater Sci Semicond Process*.**123**, 105570. (DOI: https://doi.org/10.1016/j.mssp.2020.105570)

[12] Hanif, M. A., Lee, I., Akter, J., Islam, M. A., Zahid, A. A. S. M., Sapkota, K. P. (2019). Enhanced photocatalytic and antibacterial performance of ZnO nanoparticles prepared by an efficient thermolysis method, *Catalysts*. **9**(7), 608. (DOI: https://doi.org/10.3390/catal9070608)

[13] Clavero, C. (2014). Plasmon-induced hot-electron generation at nanoparticle/metal-oxide interfaces for photovoltaic and photocatalytic devices. *Nat Photonics*, **8**(2), 95–103. (DOI: https://doi.org/10.1038/nphoton.2013.238

[14] Geldasa, F. (2024). Effect of annealing temperature on PbO thin films deposited by chemical bath deposition. *Appl Phys A*, 130. (DOI: https://doi.org/10.1007/s00339-023-07254-0)

[15] Geldasa, F. T., Kebede, M. A., Shura, M. W., Andoshe, D. M., Tegegne, N. A., Hone, F. G. (2023). Facile synthesis of different metals doped α-PbO nanoparticles for photocatalytic degradation of Methylene Blue dye, *Phys Scr*, **98**(6), 65701. (DOI: https://dx.doi.org/10.1088/1402-4896/acd0e3)

[16] Netzahual-Lopantzi, A., García-Nieto, E., Juárez-Santacruz, L., Romero-Ibarra, I. C. (2023). Photocatalytic evaluation of tetragonal and orthorhombic lead oxide nanoparticles in dye degradation treatment. *Appl Phys A*, **129**(8), 592. (DOI: https://doi.org/10.1007/s00339-023-06871-z)

[17] Borhade, A. V., Tope, D. R., Uphade, B. K. (2012). An Efficient Photocatalytic Degradation of Methyl Blue Dye by using Synthesised PbO Nanoparticles. *J Chem*, **9**(2), 362680. (DOI: https://onlinelibrary.wiley.com/doi/abs/10.1155/2012/362680)

[18] Pan, F., Raza, J., Khan, M., Ragab, A. H., Lei, T., Rafique, M. S. (2023). Preparation and structural investigations of the composite containing lead oxide and graphite as reinforcements and its adsorptive and photocatalytic dye-degradation activity. *Diam Relat*

Mater, **137**, 110170.
(DOI: https://www.sciencedirect.com/science/article/pii/S0925963523004958)

[19] Elango, G., Roopan, S. M. (2015). Green synthesis, spectroscopic investigation and photocatalytic activity of lead nanoparticles. *Spectrochim Acta Part A Mol Biomol Spectrosc*. **139**, 367–73.
(DOI: https://www.sciencedirect.com/science/article/pii/S1386142514018460)

[20] Pandiyan, R., Rajagopal, R. (2023). Fabrication and characterisation of silver and lead nanoparticles and application upon synthetic azo dye degradation. *Biomass Convers Biorefinery*, 1-6.
(DOI: https://doi.org/10.1007/s13399-023-04073-4)

[21] Nasir, G., Batool, F., Iqbal, S., Akbar, J., Noreen, S., Munawar, K. S. (2025). Biosynthesis of lead oxide nanoparticles using mulberry leaf extract for adsorptive removal of diazine black dye. *Biomass Convers Biorefinery*, **15**(8), 12525–49.
(DOI: https://doi.org/10.1007/s13399-024-06208-7)

[22] Ghalwa, N. A., Abu-Shawish, H. M., Tamous, H. M., Harazeen, H. A. (2013). Determination of electrochemical degradation of E102 dye at lead dioxide-doped carbon electrodes using some potentiometric and spectrophotometric methods. *Chem. J*, **3**(1), 1-6.
(DOI: https://onlinelibrary.wiley.com/doi/abs/10.1155/2013/691763)

[23] Wang, Z., Deb, A., Srivastava, V., Iftekhar, S., Ambat, I., Sillanpää, M. (2019). Investigation of textural properties and photocatalytic activity of PbO/TiO2 and Sb2O3/TiO2 towards the photocatalytic degradation Benzophenone-3 UV filter. *Sep Purif Technol*, **228**, 115763.
(DOI: https://www.sciencedirect.com/science/article/pii/S1383586619318404)

[24] Asgharinezhad, A. A., Rezvani, M., Ebrahimzadeh, H., Shekari, N., Ahmadinasab, N., Loni, M. (2015). Solid phase extraction of Pb (II) and Cd (II) ions based on murexide functionalized magnetic nanoparticles with the aid of experimental design methodology, Anal Methods, **7**(24), 10350–8.
(DOI: https://doi.org/10.1039/C5AY02362A)

[25] Ekinci, S., İlter, Z., Ercan, S., Çınar, E., Çakmak, R. (2021). Magnetite nanoparticles grafted with murexide-terminated polyamidoamine dendrimers for removal of lead (II) from aqueous solution: synthesis, characterization, adsorption and antimicrobial activity studies, Heliyon, **7**(3).
(DOI: https://doi.org/10.1016/j.heliyon.2021.e06600)

[26] Shahi, D. K., Regmi, S. R., Shawad, N. P., Khan, N. H., Joshi, P. R., Khatiwada, L. N., Adhikari, R. (2024). Solar-light Driven Degradation of Methylene Blue by Titanium Oxide Nanoparticles (TiO_2 NPs). *J Phys Life Sci*, **1**(1), 21–37.
(DOI: https://doi.org/10.3126/jopls.v1i1.78964)

[27] Regmi, S. R., Khan, N. H., Shawad, N. P., Shahi, D. K., Joshi, P. R., Chetry, A. B., ... (2024). Synthesis of Tin Oxide Nanoparticles (SnO_2 NPs) and its Application in the Photocatalytic Degradation of Waste Alizarin DYE. *J Phys Life Sci.* **1**(1), 38–52.

(DOI: https://doi.org/10.3126/jopls.v1i1.78982)

[28] Shi, J., Guo, P., Liu, Y., Su, J., Guo, L. (2016). PbO-sensitized ZnO nanorod arrays for enhanced visible-light-driven photoelectrochemical performance. *J Mater Res*, **31**(11), 1622–1630.
(DOI: https://doi.org/10.1557/jmr.2016.150)

[29] Yousefi, R., Khorsand Zak, A., Jamali-Sheini, F., Huang, N. M., Basirun, W. J., Sookhakian, M. (2014). Synthesis and characterization of single crystal PbO nanoparticles in a gelatin medium. *Ceram Int.* **40**(8, Part A), 11699–703.
(DOI: https://www.sciencedirect.com/science/article/pii/S0272884214005215)

[30] Makuła, P., Pacia, M., Macyk, W. (2018). How To Correctly Determine the Band Gap Energy of Modified Semiconductor Photocatalysts Based on UV–Vis Spectra. *J Phys Chem Lett*, **9**(23), 6814–7.
(DOI: https://doi.org/10.1021/acs.jpclett.8b02892)

[31] Piro, S. J., Hamad, S. M., Barzinjy, A. A., Abdullah, B. J., Omar, M. S., Shaikhah, D. (2023). Green tea extract mediated biosynthesis of lead oxide nanoparticles: characterization, and catalytical activity. Bioresour Technol Reports. **24**, 101612,
(DOI: https://www.sciencedirect.com/science/article/pii/S2589014X23002839)

[32] Nafees, M., Ikram, M., Ali, S. (2017). Thermal stability of lead sulfide and lead oxide nano-crystalline materials. *Appl Nanosci*, **7**(7), 399–406.
(DOI: https://doi.org/10.1007/s13204-017-0578-7)

[33] Li, M., Shao, Z., Li, Z., Zhu, D., Wang, J., Karazhanov, S. Z., ... (2023). Co-Sputtering Crystal Lattice Selection for Rare Earth Metal-Based Multi Cation and Mixed Anion Photochromic Films. *Nanomaterials*, **13**(4).
(DOI: https://www.mdpi.com/2079-4991/13/4/684)

[34] Senvaitiene J., Smirnova, J., Beganskiene, A., Kareiva, A. (2007). XRD and FTIR Characterisation of Lead Oxide-Based Pigments and Glazes. *Acta Chim Slov.* **54**(1).

[35] Mahalingam, T, Velumani S, Raja M, Thanikaikarasan S, Chu JP, Wang SF, et al. (2007). Electrosynthesis and characterization of lead oxide thin films, Mater Charact. **58**(8–9), 817–22.
(DOI: https://doi.org/10.1016/j.matchar.2006.11.021)

[36] Moreno-Tovar, R., Terrés, E., Rangel-Mendez,. J. R. (2014). Oxidation and EDX elemental mapping characterization of an ordered mesoporous carbon: Pb (II) and Cd (II) removal. *Appl Surf Sci*. **303**, 373–80.
(DOI: https://doi.org/10.1016/j.apsusc.2014.03.008)

[37] Helali, S., Rashad, M., Ben Mabrouk, A., Alanazi, M. A. A., Mustafa, M. S. (2024). Structural Analysis and Adsorption Studies of (PbO, MgO) Metal Oxide Nanocomposites for Efficient Methylene Blue Dye Removal from Water. *Materials*, **17**(12).
(DOI: https://www.mdpi.com/1996-1944/17/12/2890)

[38] Yazdani-Darki, S., Eslami-Kalantari, M., Zare, H. (2021). Study of double-using ultrasonic effects on the structure of PbO nanorods fabricated by the sonochemical method, *Ultrason*

Sonochem. **79**, 105797.
((DOI: https://doi.org/10.1016/j.ultsonch.2021.105797)

[39] Patterson, A. L. (1939). The Scherrer Formula for X-Ray Particle Size Determination. *Phys Rev*, **56**(10), 978–82.
(DOI: https://link.aps.org/doi/10.1103/PhysRev.56.978)

[40] Park, S., Baker, J. O., Himmel, M. E., Parilla, P. A., Johnson, D. K. (2010). Cellulose crystallinity index: measurement techniques and their impact on interpreting cellulase performance. *Biotechnol Biofuels*, **3**(1), 10.
(DOI: https://doi.org/10.1186/1754-6834-3-10)

[41] Momma, K., Izumi, F. (2008). VESTA: a three-dimensional visualization system for electronic and structural analysis. *J Appl Crystallogr*, **41**(3), 653–8.
(DOI: https://doi.org/10.1107/S0021889808012016)

[42] Hanif, M. A., Akter, J., Lee, I., Islam, M. A., Sapkota, K. P., Abbas, H. G. Hahn, J. R. (2021). Formation of chemical heterojunctions between ZnO nanoparticles and single-walled carbon nanotubes for synergistic enhancement of photocatalytic activity. *J Photochem Photobiol A Chem*. 413,113260.
(DOI:https://www.sciencedirect.com/science/article/pii/S1010603021001325)

[43] Alagar, M., Theivasanthi, T. and Raja, A. K. (2012). Chemical synthesis of nano-sized particles of lead oxide and their characterization studies. *arXiv preprint arXiv*, 1204, 0896.
(DOI: https://doi.org/10.3923/jas.2012.398.401)

[44] Mythili, N., & Arulmozhi, K. T. (2014). Characterization studies on the chemically synthesized α and β phase PbO nanoparticles. *Int. J. Sci. Eng. Res.*,**5**(1), 412-416.

[45] Herrmann, J. M. (1999). Heterogeneous photocatalysis: fundamentals and applications to the removal of various types of aqueous pollutants. *Catalysis today*, 53(1), 115-129.
(DOI: https://doi.org/10.1016/S0920-5861(99)00107-8)

[46] Langmuir, I. (1918). The adsorption of gases on plane surfaces of glass, mica and platinum. *Journal of the American Chemical society*, **40**(9), 1361-1403.
(DOI: https://doi.org/10.1021/ja02242a004)

[47] Haleem, A., Shafiq, A., Chen, S.-Q., & Nazar, M. (2023). A Comprehensive Review on Adsorption, Photocatalytic and Chemical Degradation of Dyes and Nitro-Compounds over Different Kinds of Porous and Composite Materials. *Molecules*, **28**(3), 1081.
(DOI; https://doi.org/10.3390/molecules28031081).